CHAPTER VI

CONCLUSION AND SUGGESTION

6.1 Conclusion

This study implemented the application of the Coupled Eulerian-Lagrangian (CEL) method to investigate the landmass runout kinematic behaviour of Aso-Bridge landslide - slope failure and its deposition process. The slope was employed as an elastoplastic geomaterial constitutive model in explicit algorithm integration using commercial finite element software, ABAQUS. The simulations results show that Coupled Eulerian-Lagrangian (CEL) formulation is stable and able to demonstrate the landmass transport large deformation with convergent results. The proposed simulation indicates that the meshing size and friction coefficient contribute a strong influence on the landmass runout. The models simulated with the same friction coefficient have different results when the meshing sizes were different. That with larger meshing size of 20 unit mesh, has the landmass already deform even at t = 0s, while that with smaller meshing size of 3,2 unit mesh gave a more reliable and realistic visual illustration of the deposition process. The friction coefficient affects the transportation process of the landmass, including the velocity and the amount of mass deposited in the river bank by the end of the simulation. Smaller friction coefficient will give a higher velocity and more amount of landmass transported at the respected time. Based on the analysis, the friction coefficient of μk = 1 gave

better agreement in term of results with those published for the previous study.

6.2 Suggestion

The friction coefficient used in the simulation was based on the empirical approach from previous studies. Further studies are expected to formulate friction coefficients for cases with various specific conditions. The effect of topography (surface roughness) is also suggested to be considered to understand the more precise evolution process of the landslide.

REFERENCES

Ugai K, Leshchinsky D, 1995, Three-dimensional limit equilibrium and finite element analyses: a comparison of results. Soils Found 35(4):1–7.

Khosravi M, Khabbazian M, 2012, presentation of critical failure surface of slopes based on the finite element technique. Pro2014ceedings of Geocongress: state of the art and practice in geotechnical engineering, American Society of Civil Engineers, Reston, VI (2012):536–545.

Hung C, Lin GW, Syu HS, Chen CW, Yen HY, 2017, Analysis of the Aso-bridge landslide during the 2016 Kumamoto earthquakes in Japan. Bull Eng Geol Environ. https://doi.org/10.1007/s10064-017-1103-7

Zhou JW, Cui P, Yang XG, 2013, Dynamic process analysis for the initiation and movement of the Donghekou landslide-debris flow triggered by the Wenchuan earthquake. J Asian Earth Sci 76:70–84.

Bishop AW, 1955, The use of the slip circle in the stability analysis of slopes. Geotechnique 5(1):7–17.

Hung C, Liu Chi- Hsuan, Lin Guan-Wei, Leshchinsky Ben, 2018, The Aso-Bridge coseismic landslide: a numerical investigation of failure and runout behavior using finite and discrete element methods. Bulletin of Engineering Geology and the Environment. https://doi.org/10.1007/s10064-018-1309-3.

Duncan JM, 1996, State of the art: limit equilibrium and finite-element analysis of slopes. J Geotech Geoenviron 122(7):577–596.

Spencer E, 1967, A method of analysis of the stability of embankments assuming parallel inter-slice forces. Geotechnique 17(1):11–26.

Mendjel D, Messast S, 2012, Development of limit equilibrium method as optimization in slope stability analysis. Struct Eng Mech 41(3): 339–348.

Chen Xiang Yu, Zhang Lulu, Chen Lihong, Li Xu, Liu Dongsheng, 2018, Slope stability analysis based on the Coupled Eulerian-Lagrangian finite element method. Bulletin of Engineering Geology and the Environment. https://doi.org/10.1007/s10064-018-1413-4

Liu SY, Shao LT, Li HJ, 2015, Slope stability analysis using the limit equilibrium method and two finite element methods. Comput Geotech 63(63):291–298.

Javankhoshdel S, Luo N, Bathurst RJ, 2016, Probabilistic analysis of simple slopes with cohesive soil strength using RLEM and RFEM. Georisk: Assess Manag Risk Eng Syst Geohazards 11(3):231–246.

ABAQUS, 2014, Getting Started with ABAQUS: Interactive Edition. Version 6.14. (2014) Dassault Systèmes Simulia Corp., Providence, RI, USA.

Yuan J, Papaioannou I, Straub D, 2018, Probabilistic failure analysis of infinite slopes under random rainfall processes and spatially variable soil. Georisk: Assessment and Management of Risk for Engineered Systems and Geohazards. https://doi.org/10.1080/17499518.2018.1489059

Chen H, Lee CF, 2000, Numerical simulation of debris flow. Can Geotech J 37:146–160.

Crosta GB, Chen H, Frattini P, 2006, Forecasting hazard scenarios and implications for the evaluation of countermeasure efficiency for large debris avalanches. Eng Geol 83:236–253.

BBC, 2014, Indonesia landslide: Many missing in Java, accessed on June 15, 2019. https://www.bbc.com/news/world-asia-30459175

DW, 2016, Indonesia landslide buries dozens of people, accessed on June 15, 2019. https://www.dw.com/en/indonesia-landslide-buries-dozens-of-people/a-38249018

Abaqus 3DEXPERIENCE R2018x, 2018, 3DEXPERIENCE R2018x manuals: Course Catalog 3DEXPERIENCE R2018x / R2019x. Dassault Systèmes Simulia Corp., Providence, RI, USA.

Benson DJ, 1992, Computational methods in Lagrangian and Eulerian hydrocodes. Comput Methods Appl Mech Eng 99:235–394.

Benson DJ, 1995, A multi-material Eulerian formulation for the efficient solution of impact and penetration problems. Comput Mech 15: 558–571.

Benson DJ, Okazawa S, 2004, Contact in a multi-material Eulerian finite element formulation. Comput Methods Appl Mech Eng 193:4277– 4298.

Hirt CW, Nichols BD, 1981, Volume of fluid (VOF) method for the dynamics of free boundaries. J Comput Phys 39:201–225.

Benson DJ, 2000, An implicit multi-material eulerian formulation. Int J Numer Methods Eng 48(4):475–499.

Malvern L.E.,1969, Introduction to the Mechanics of a Continuous Medium. Prentice-Hall, Englewood Cliffs, NJ, USA.

JICA, 2015, Country Report Indonesia: Natural Disaster Risk Assessment and Area Business Continuity Plan Formulation for Industrial Agglomerated Areas in the ASEAN Region. AHA Centre Japan International Cooperation Agency, Chiyoda, Tokyo, Japan.

APPENDIX

APPENDIX A

Aso-Bridge Slope Cross-Sectional Coordinates

(*Produced using the information from: Geospatial Information Authority of Japan and Geographical Survey Institute of Japan)*

Horizontal Distance (m)	Elevation (m)	Horizontal Distance (m)	Elevation (m)
0	719	0	714
9	713	6	711
18	707	11	703
27	699	17	694
36	691	23	693
45	687	28	688
54	683	34	685
63	677	40	678
72	669	45	671
81	661	51	666
90	654	57	663
99	648	62	659
108	645	68	654
117	638	74	650
126	631	79	645
135	621	85	640
144	610	90	637
153	604	96	636
162	599	102	630
171	596	107	626
180	591	113	619
189	583	119	617
197	576	124	613
206	570	130	608
215	563	136	605
224	556	141	602
233	554	147	599
242	548	153	596
251	539	158	591
260	531	164	584
269	526	170	582
278	521	175	580
287	515	181	579
296	513	187	578
305	510	192	575
314	506	198	574

323	502	204	572
332	498	209	566
341	492	215	562
350	487	221	559
359	483	226	556
368	482	232	553
377	478	238	549
386	475	243	544
395	472	249	539
404	469	255	537
413	466	260	533
422	464	266	530
431	462	271	525
440	459	277	523
449	457	283	518
458	454	288	515
467	452	294	511
476	449	300	509
485	447	305	507
494	446	311	503
503	442	317	501
512	440	322	500
521	438	328	498
530	436	334	497
539	434	339	494
548	433	345	491
557	432	351	489
566	430	356	488
575	427	362	485
583	425	368	484
592	422	373	482
601	420	379	481
610	417	385	478
619	417	390	475
628	414	396	473
637	411	402	470
646	410	407	468
655	408	413	468
664	407	419	467
673	406	424	466
682	405	430	462
691	404	436	461
700	403	441	459
709	401	447	459

718	399	452	457
727	397	458	455
736	395	464	453
745	394	469	450
754	391	475	448
763	385	481	447
772	375	486	446
781	364	492	443
790	353	498	440
799	350	503	438
808	348	509	437
817	347	515	436
826	347	520	434
835	347	526	434
844	350	532	432
853	357	537	431
862	365	543	430
871	368	549	428
880	379	554	425
889	388	560	424
898	397	566	424
907	404	571	424
916	408	577	424
925	408	583	423
934	408	588	422
943	407	594	420
952	407	600	419
961	407	605	419
969	407	611	417
978	408	616	415
-	-	622	413
-	-	628	412
-	-	633	410
-	-	639	409
-	-	645	407
-	-	650	404
-	-	656	400
-	-	662	396
-	-	667	393
-	-	673	392
-	-	679	392
-	-	684	391
-	-	690	390
-	-	696	388

-	-	701	388
-	-	707	388
-	-	713	389
-	-	718	389
-	-	724	389
-	-	730	388
-	-	735	386
-	-	741	385
-	-	747	383
-	-	752	380
-	-	758	380
-	-	764	380
-	-	769	379
-	-	775	378
-	-	781	377
-	-	786	374
-	-	792	370
-	-	797	368
-	-	803	368
-	-	809	364
-	-	814	360
-	-	820	355
-	-	826	348
-	-	831	343
-	-	837	343
-	-	843	341
-	-	848	339
-	-	854	337
-	-	860	335
-	-	865	340
-	-	871	344
-	-	877	349
-	-	882	357
-	-	888	365
-	-	894	372
-	-	899	380
-	-	905	387
-	-	911	394
-	-	916	393
-	-	922	396
-	-	928	398
-	-	933	400
-	-	939	402
-	-	945	403

-	-	950	403
-	-	956	403
-	-	962	405
-	-	967	408
-	-	973	410
-	-	978	411

APPENDIX B: MODEL PARTS AND ASSEMBLY

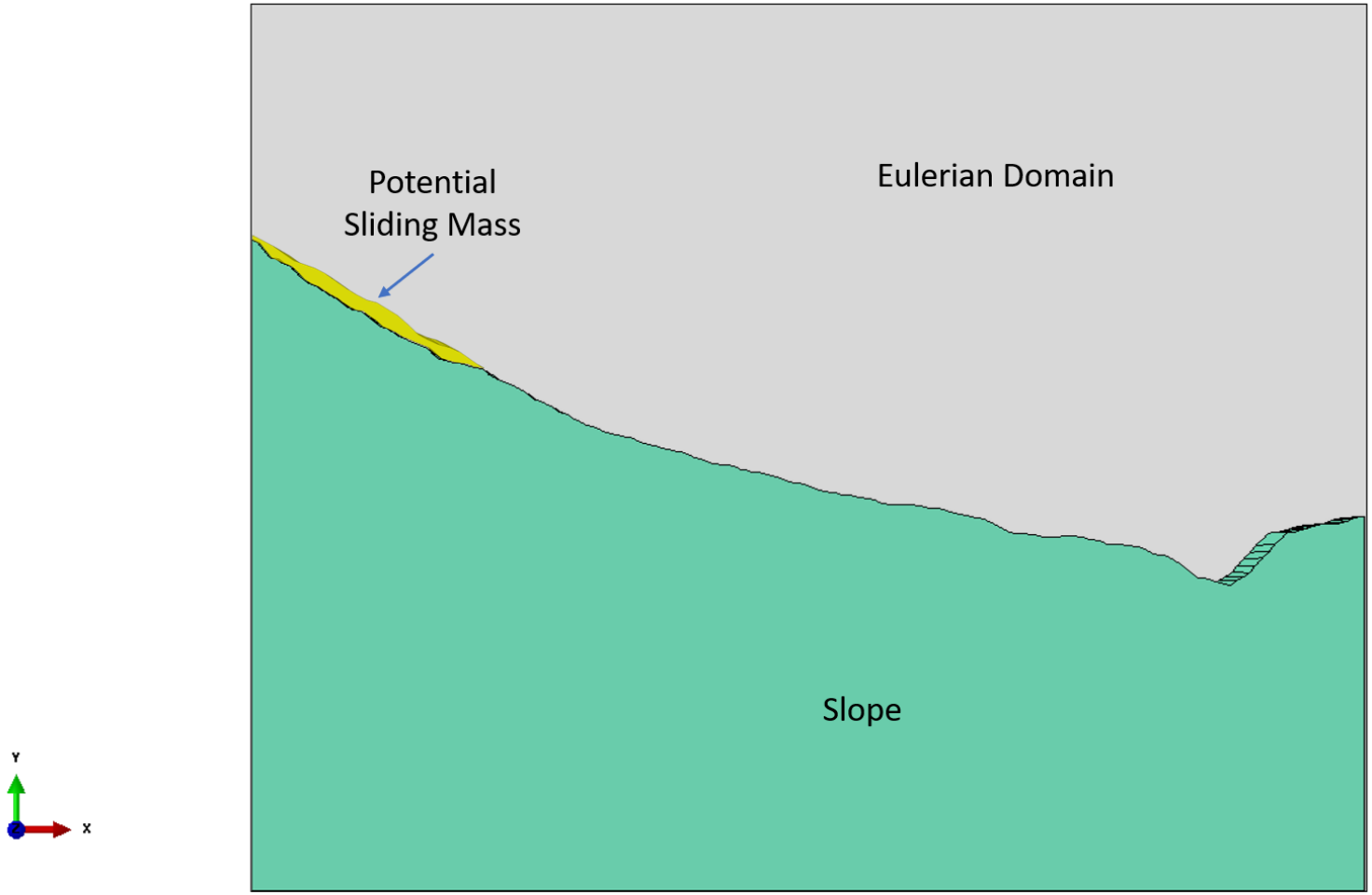

APPENDIX C: SIMULATION RESULTS – μ=0,8 MESH 20
APPENDIX C-1: t = 0 s

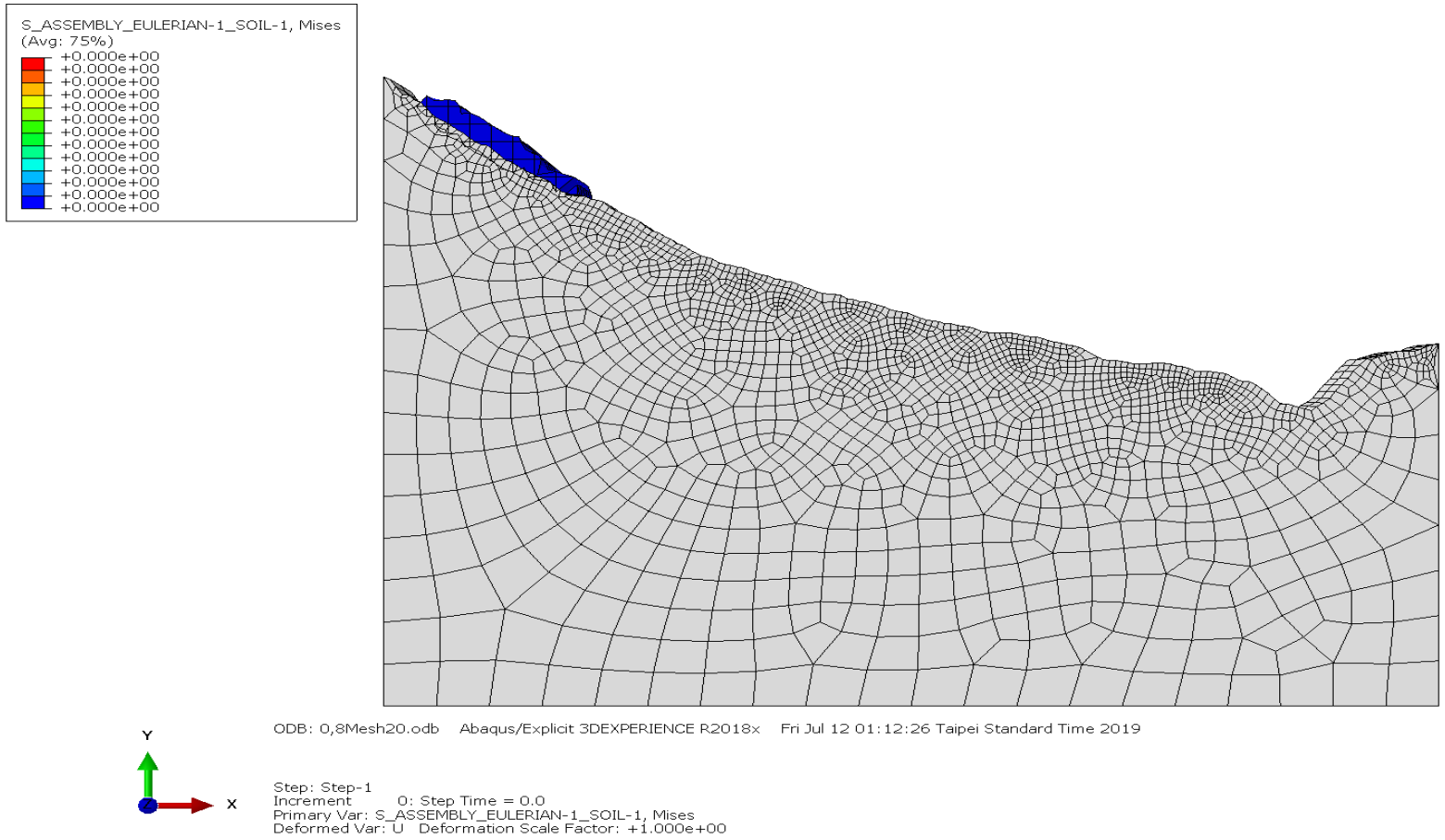

APPENDIX C-2: t = 1,9 s

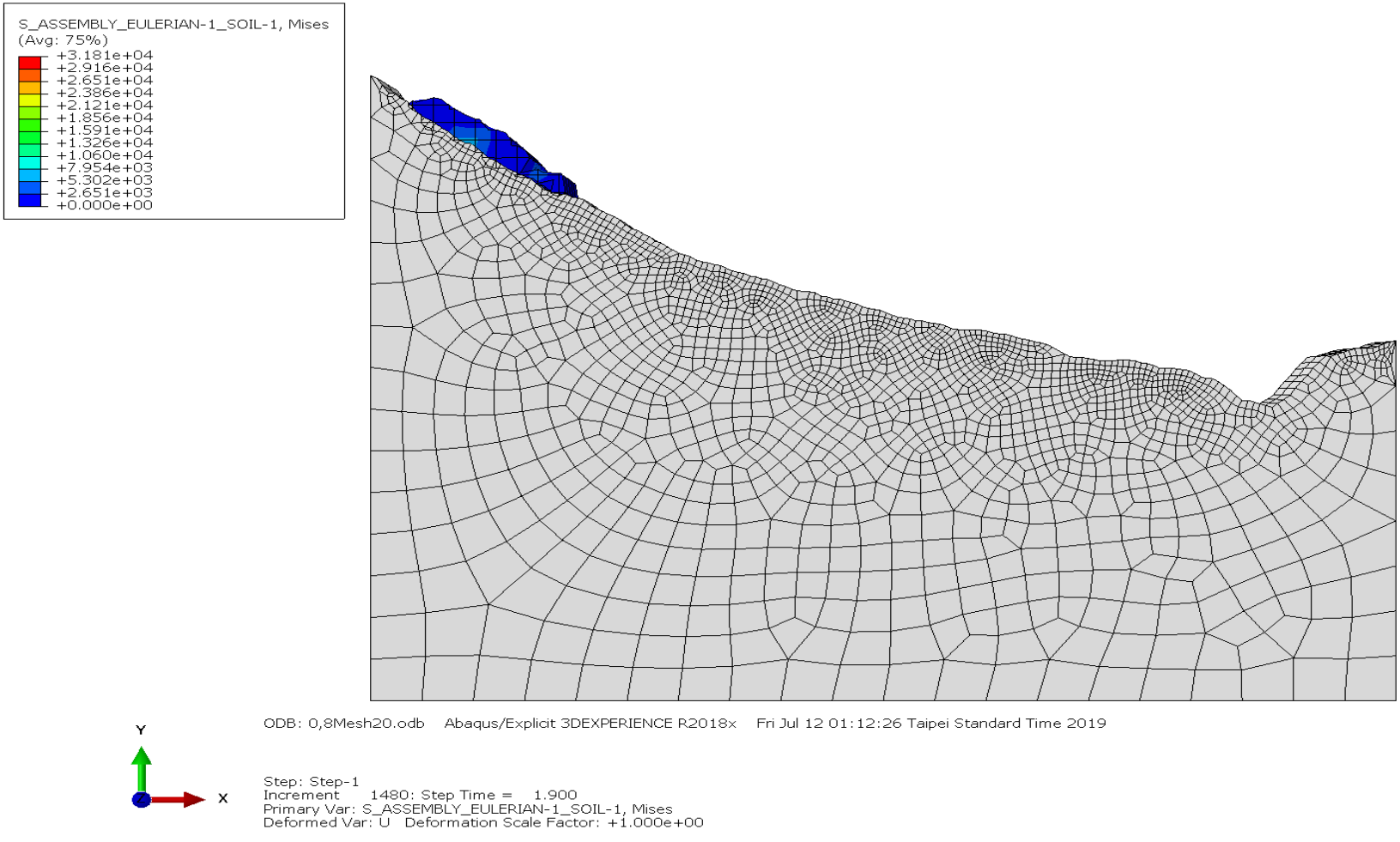

APPENDIX C-3: t = 11,40 s

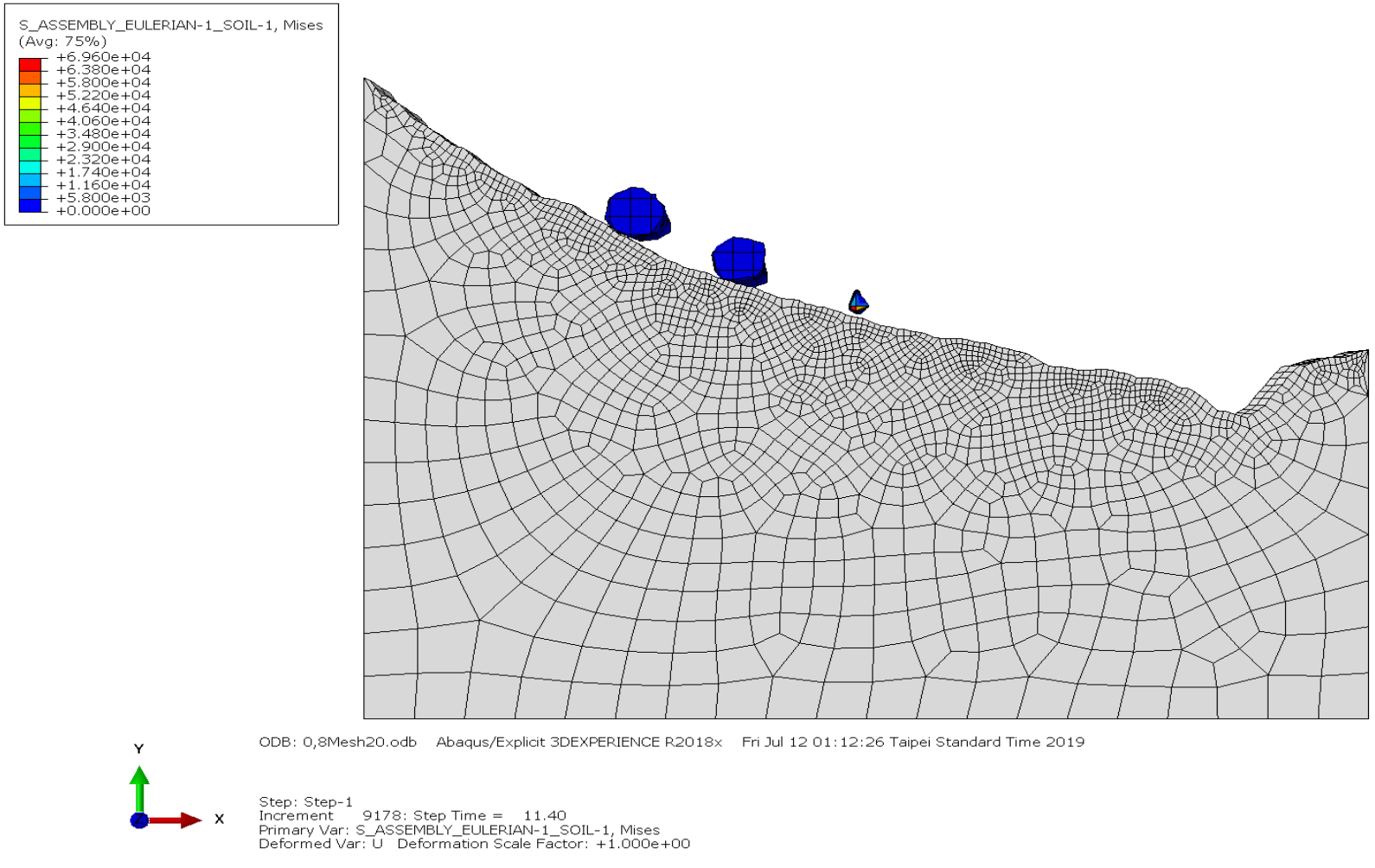

APPENDIX C-4: t = 19 s

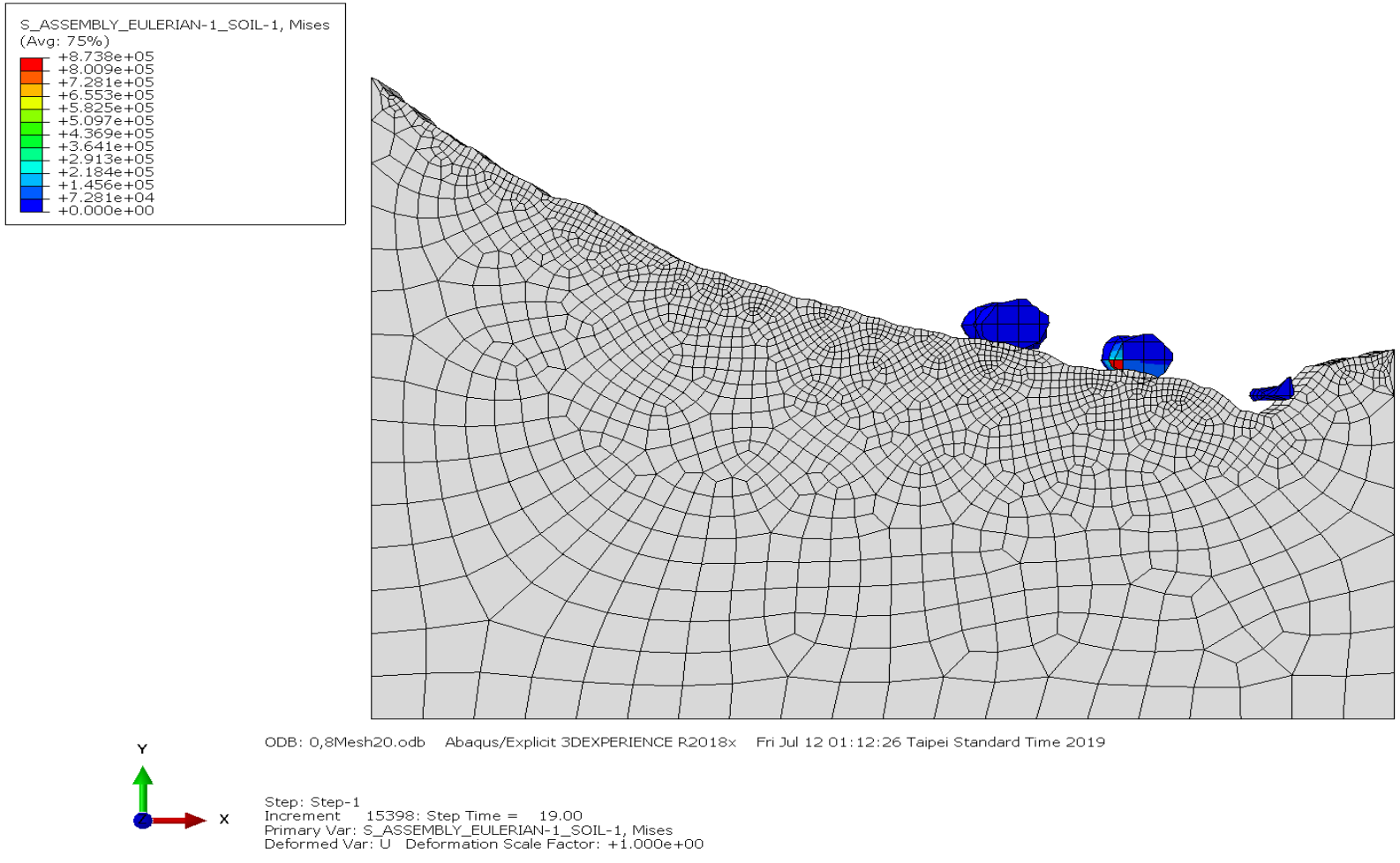

APPENDIX C-5: t = 20,90 s

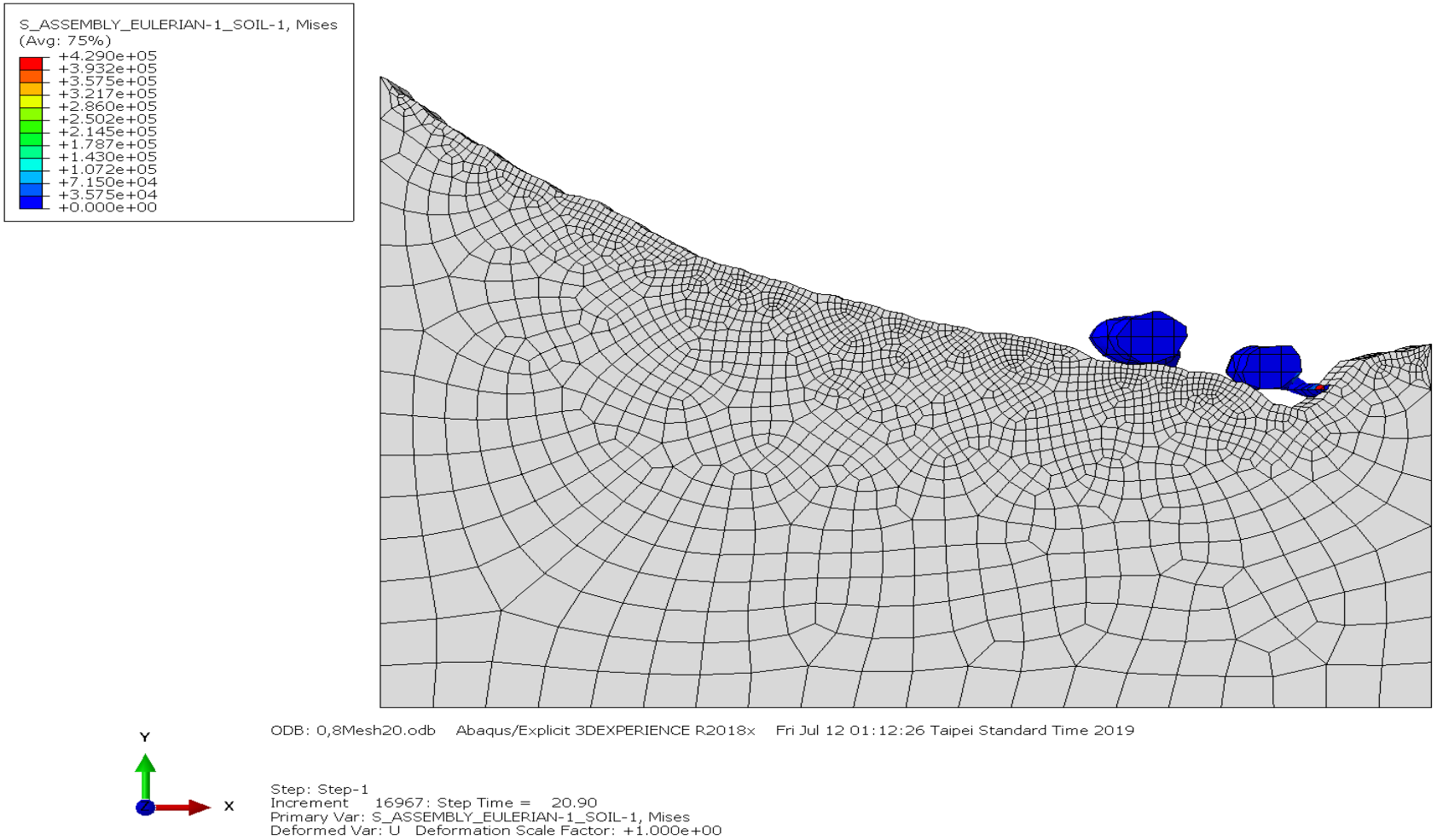

APPENDIX C-6: t = 38 s

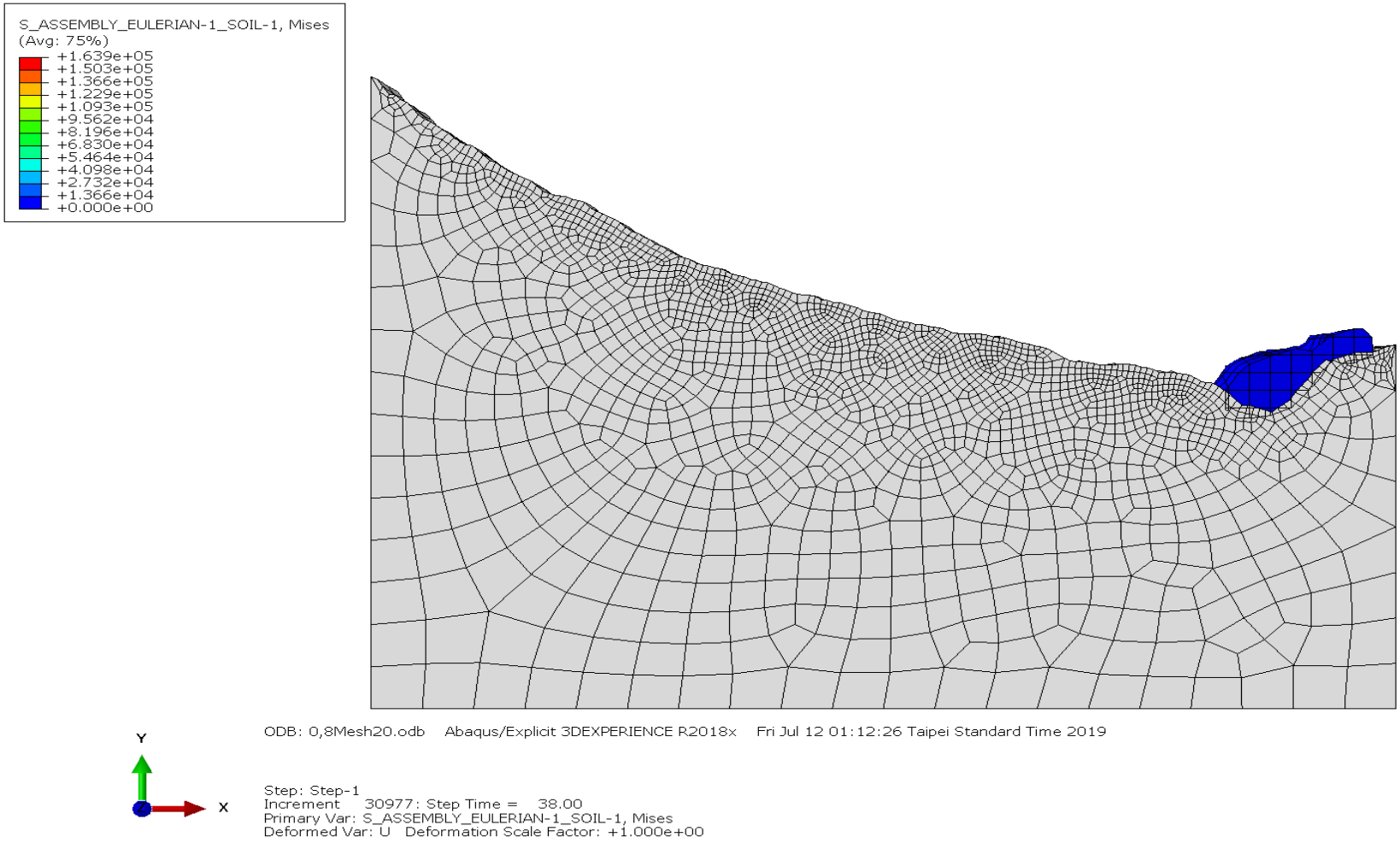

APPENDIX D: SIMULATION RESULTS – μ=0,8 MESH 3,2
APPENDIX D-1: t = 0 s

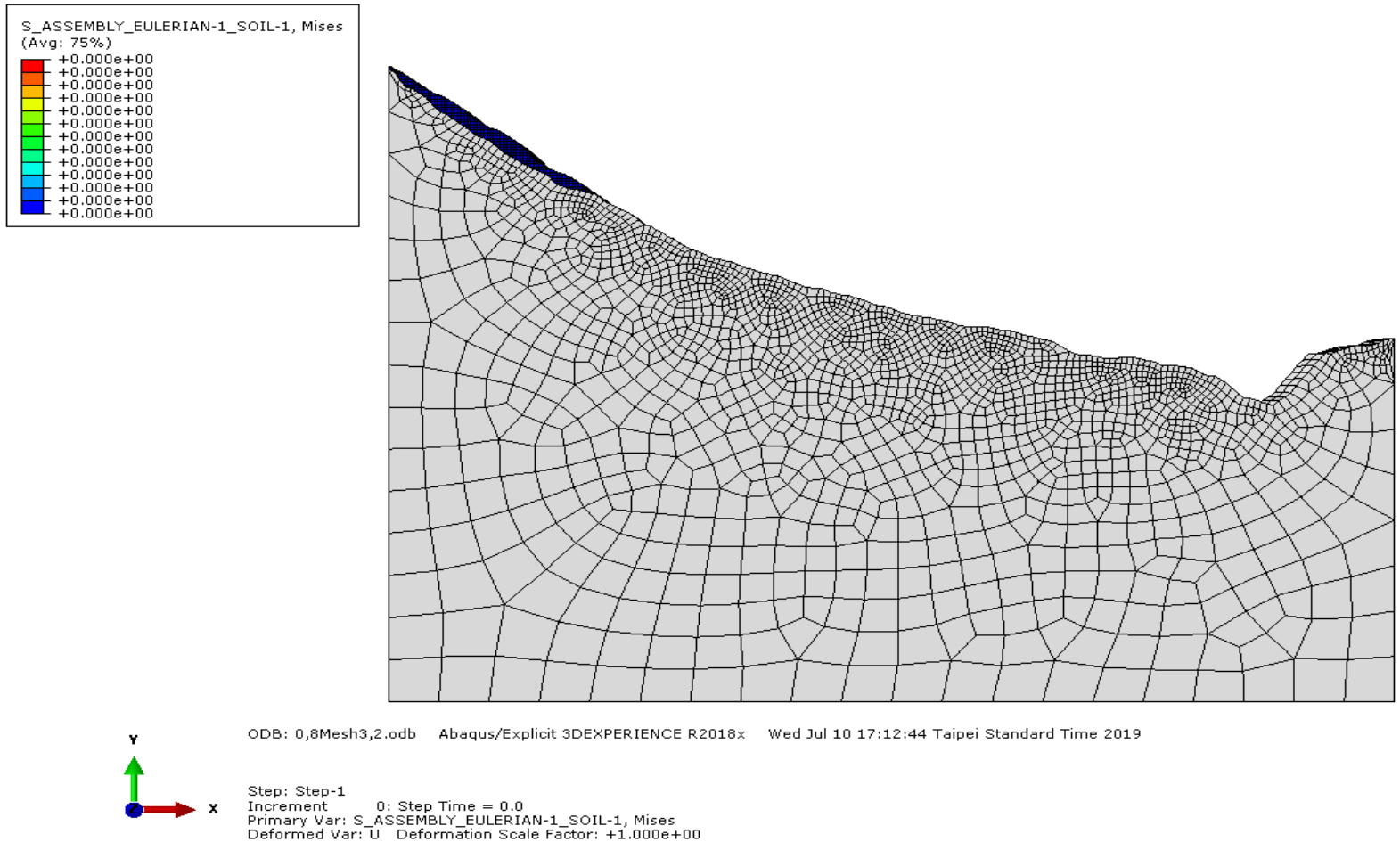

APPENDIX D-2: t = 1,9 s

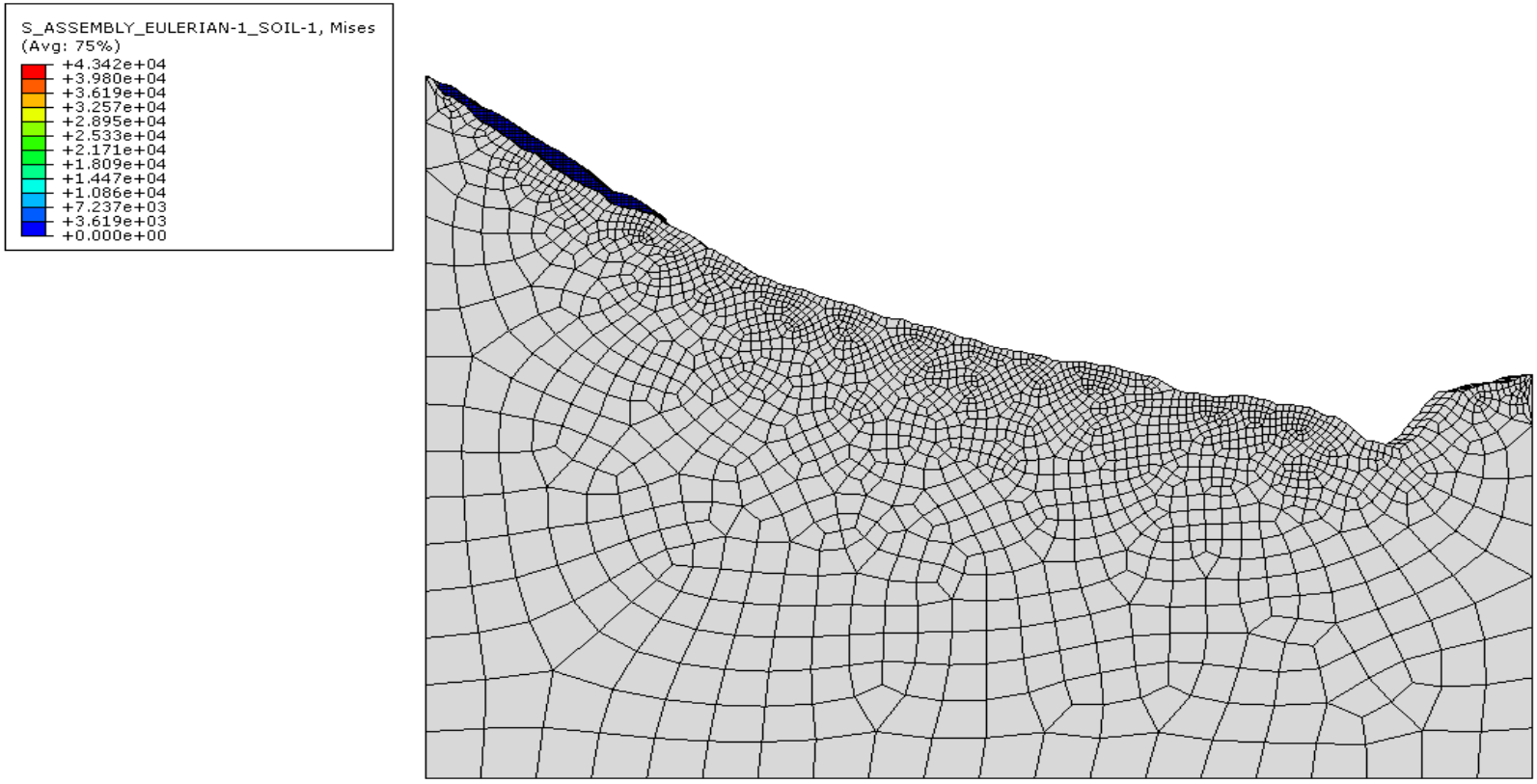

APPENDIX D-3: t = 7,6 s

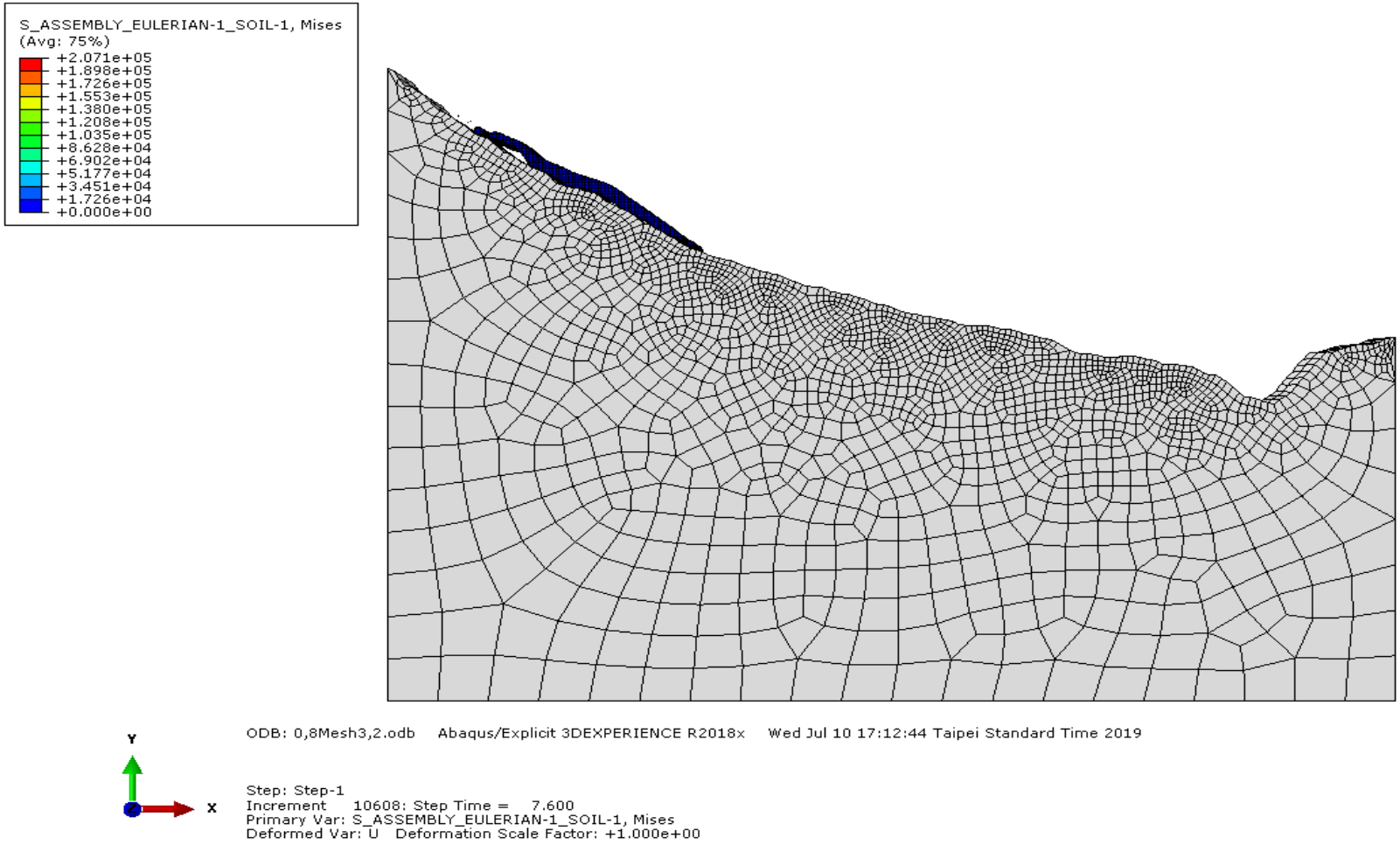

APPENDIX D-4: t = 11,40 s

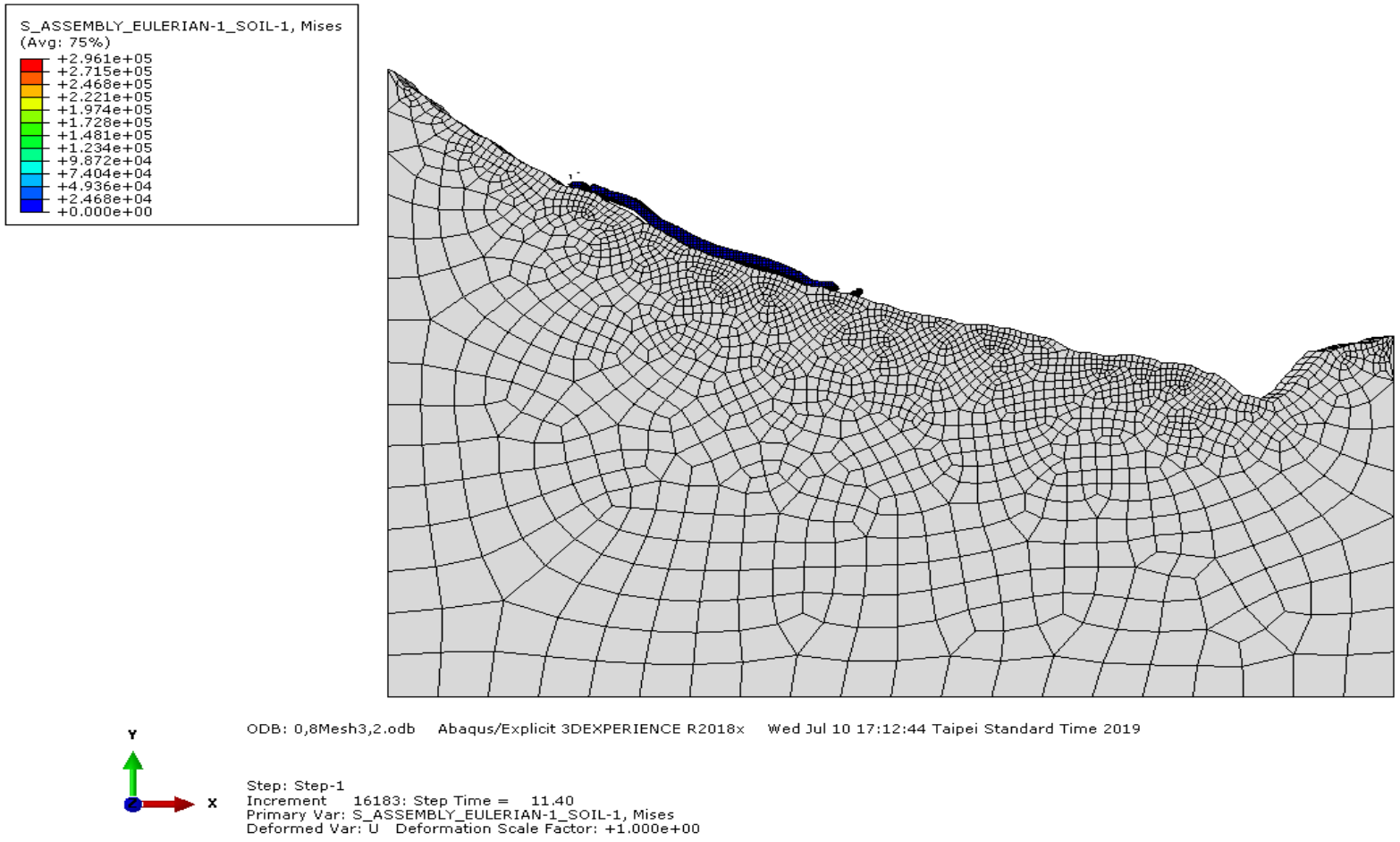

APPENDIX D-5: t = 19 s

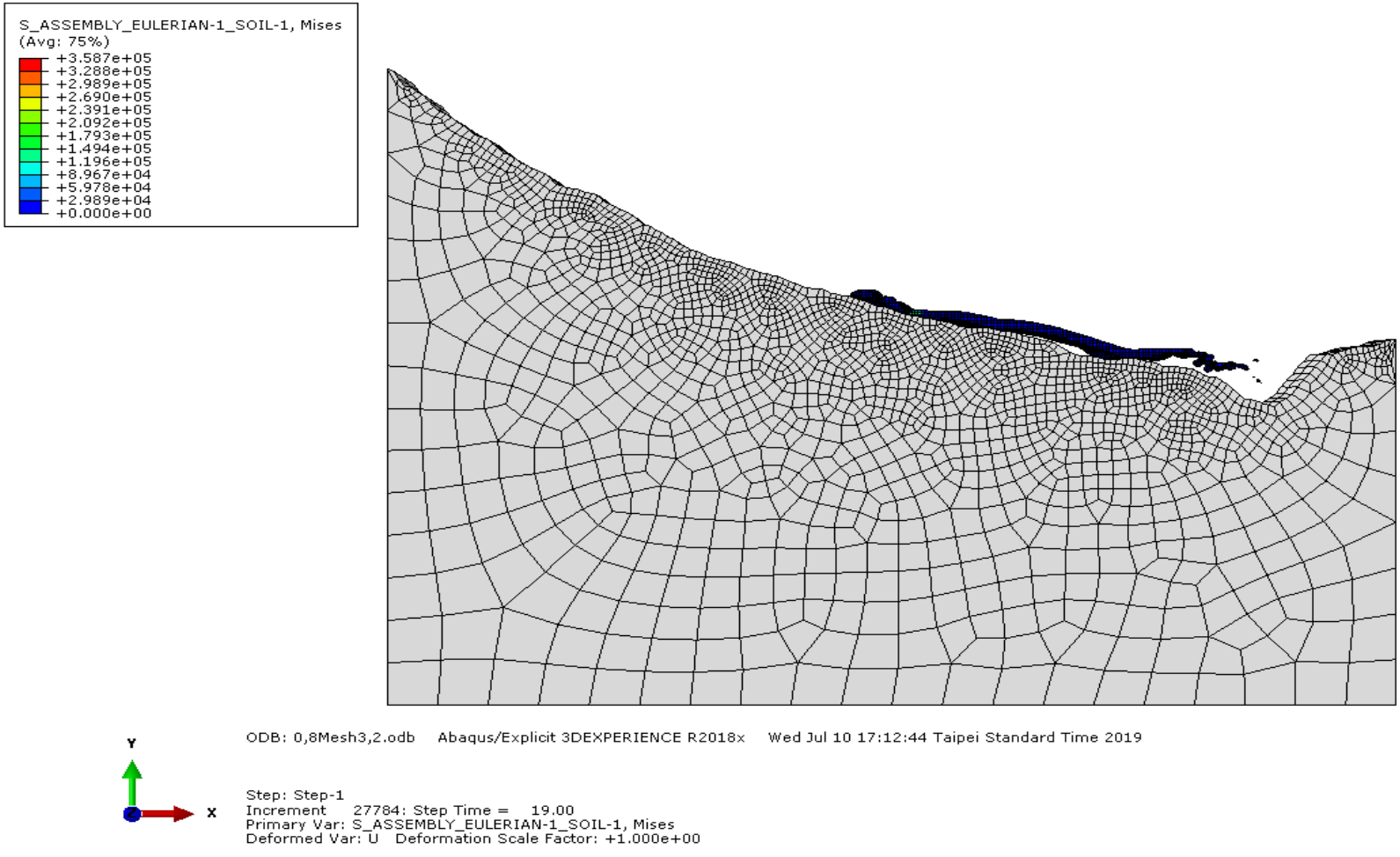

APPENDIX D-6: t = 20,90 s

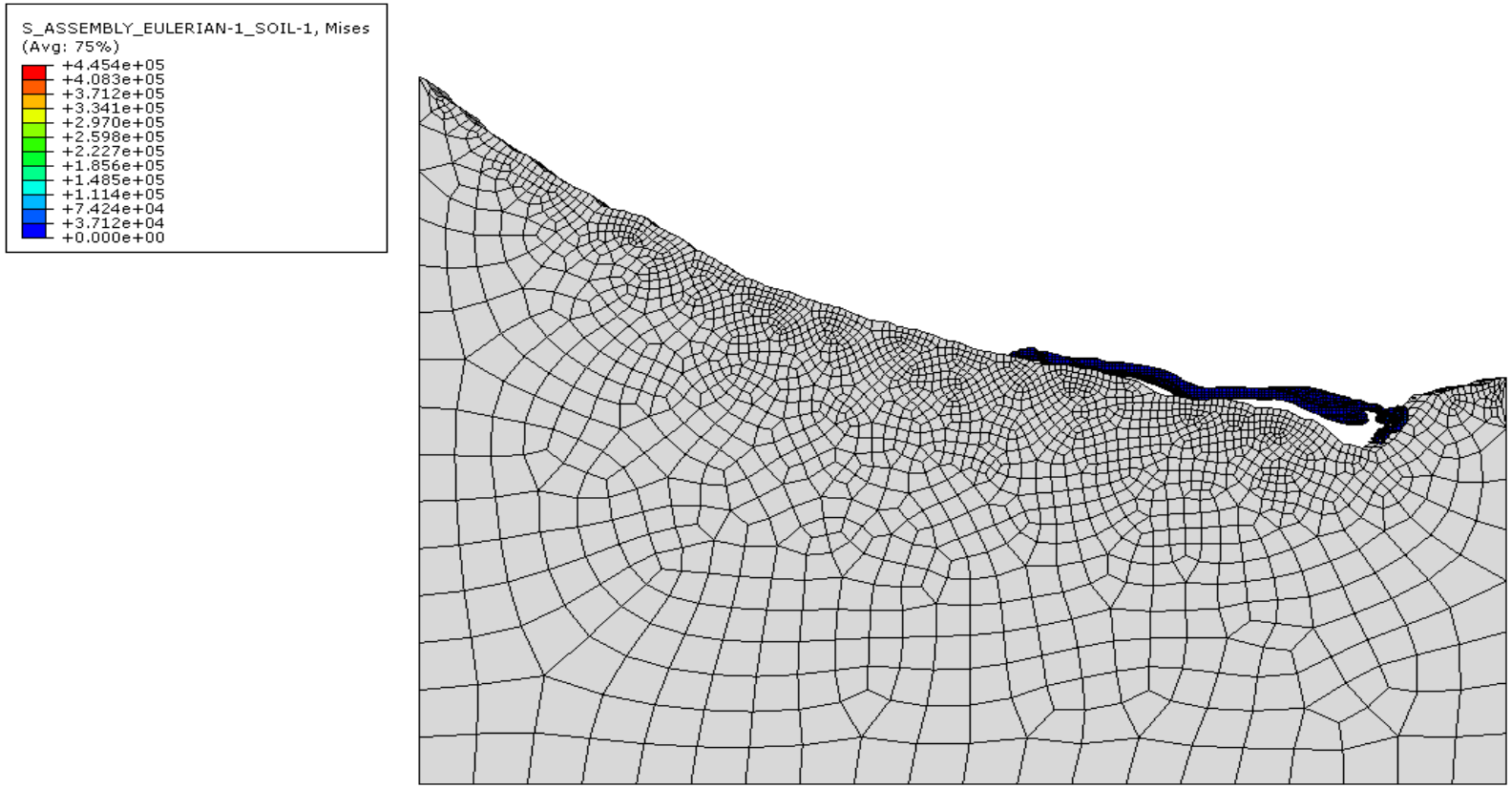

APPENDIX D-7: t = 38 s

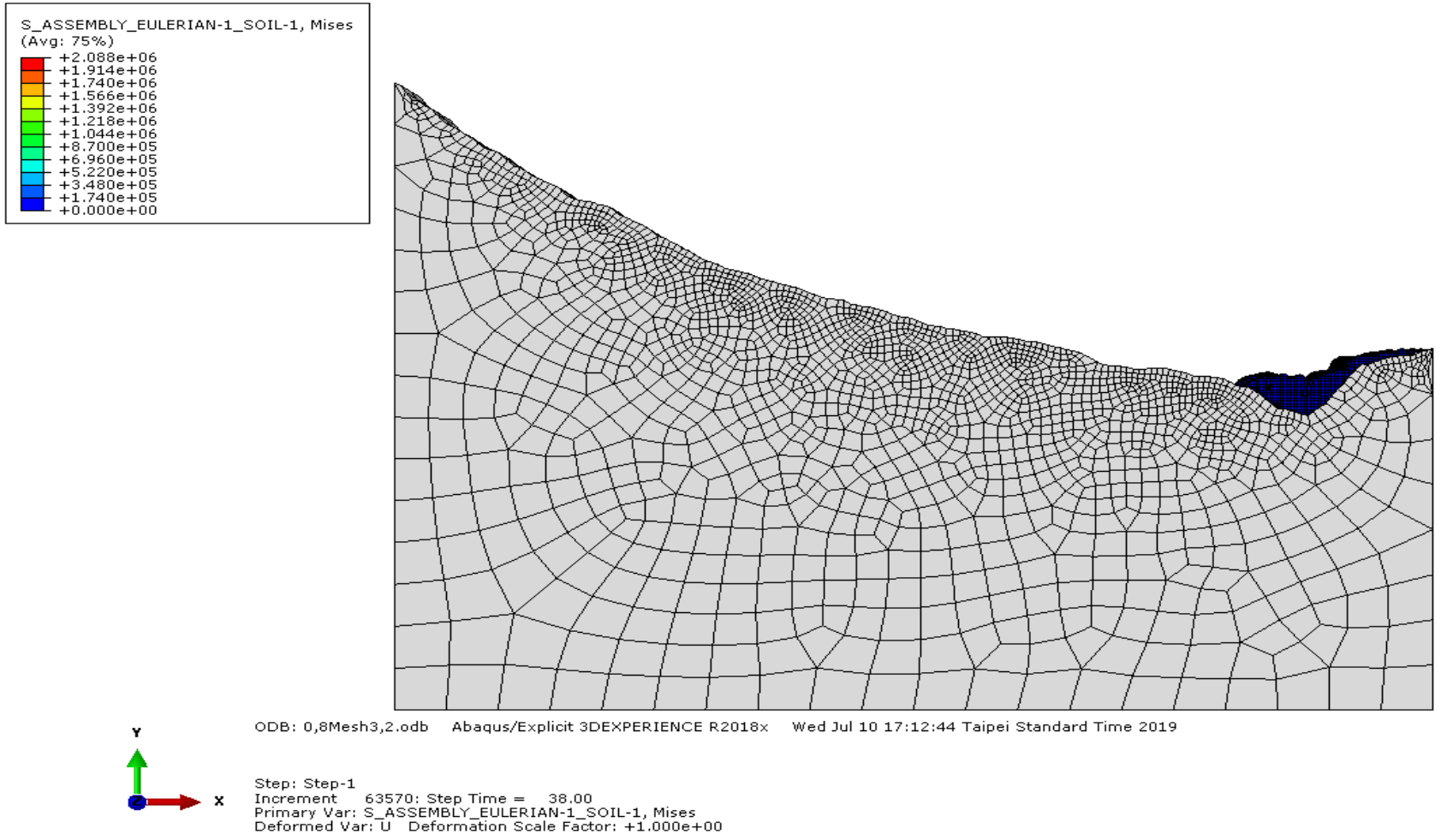

APPENDIX E: SIMULATION RESULTS – μ=1 MESH 3,2
APPENDIX E-1: t = 0 s

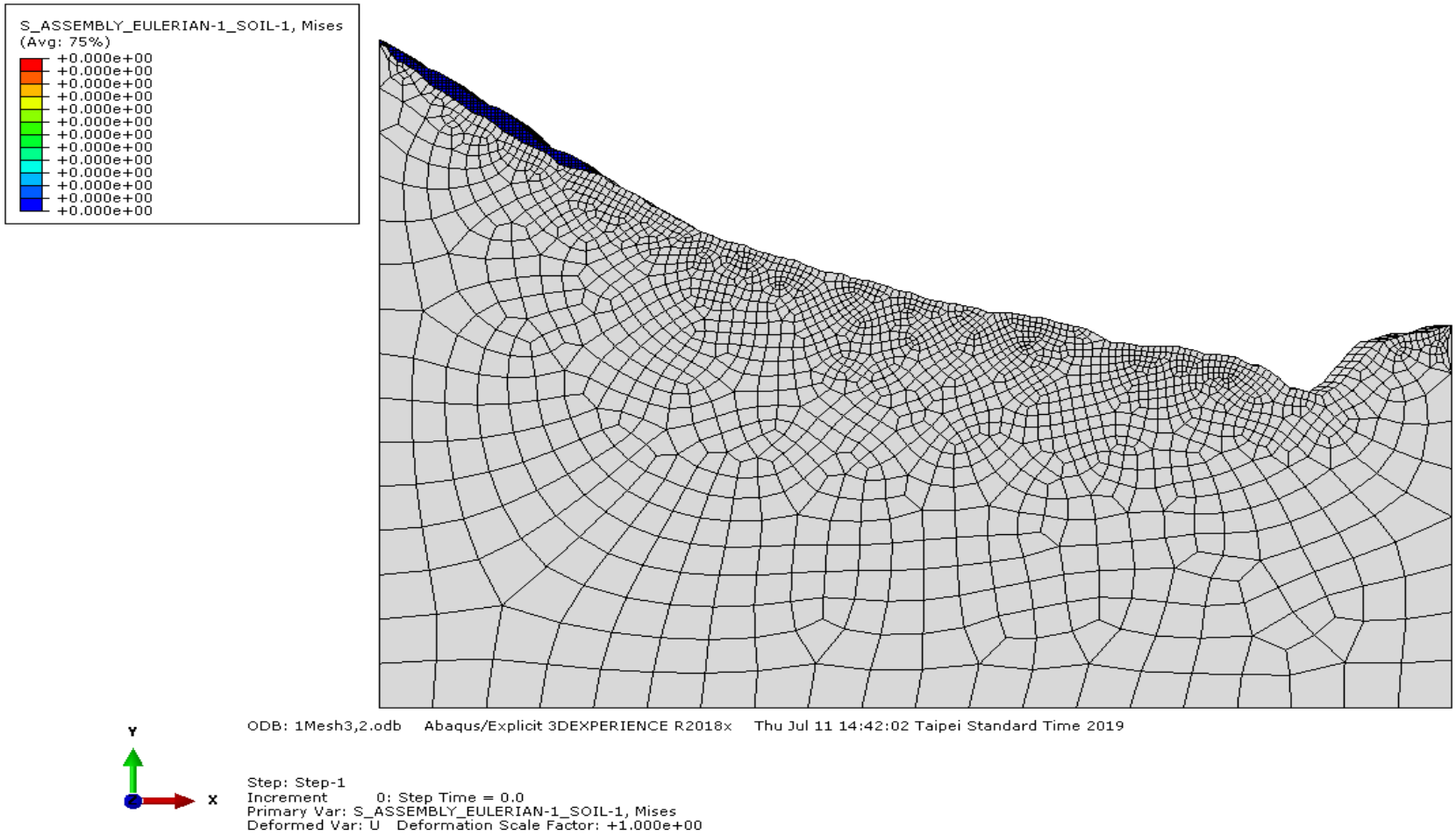

APPENDIX E-2: t = 1,9 s

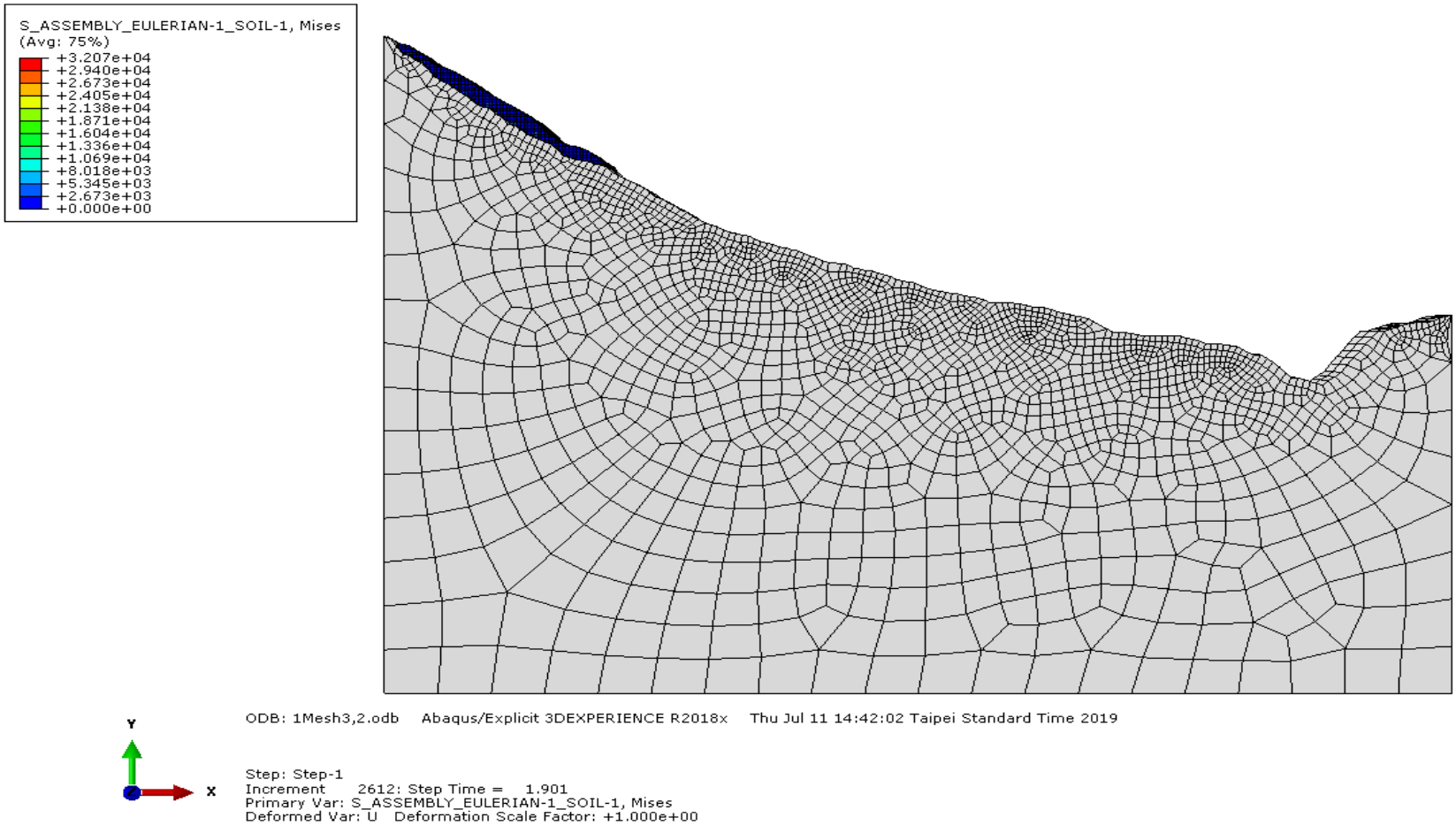

APPENDIX E-3: t = 7,6 s

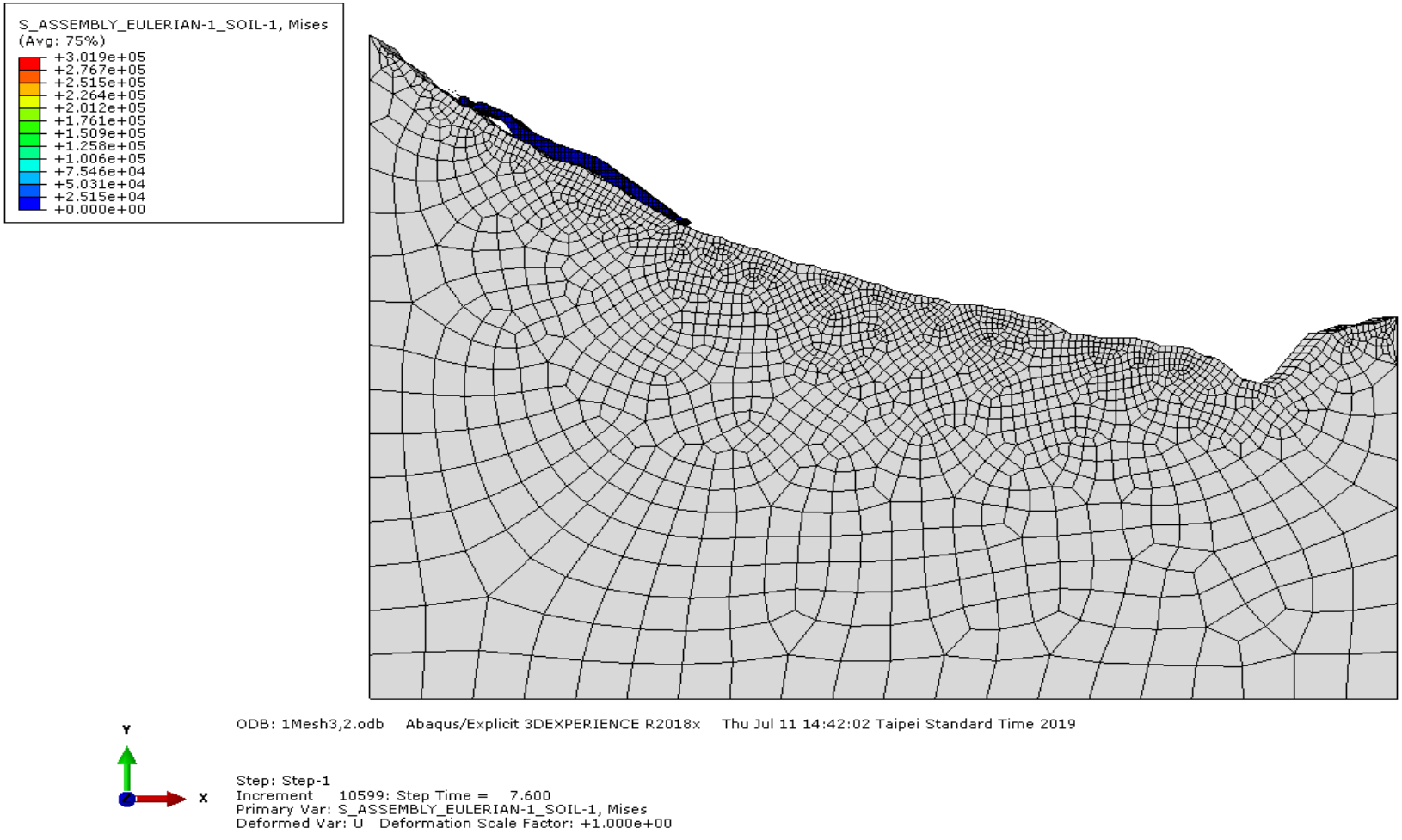

APPENDIX E-4: t = 11,40 s

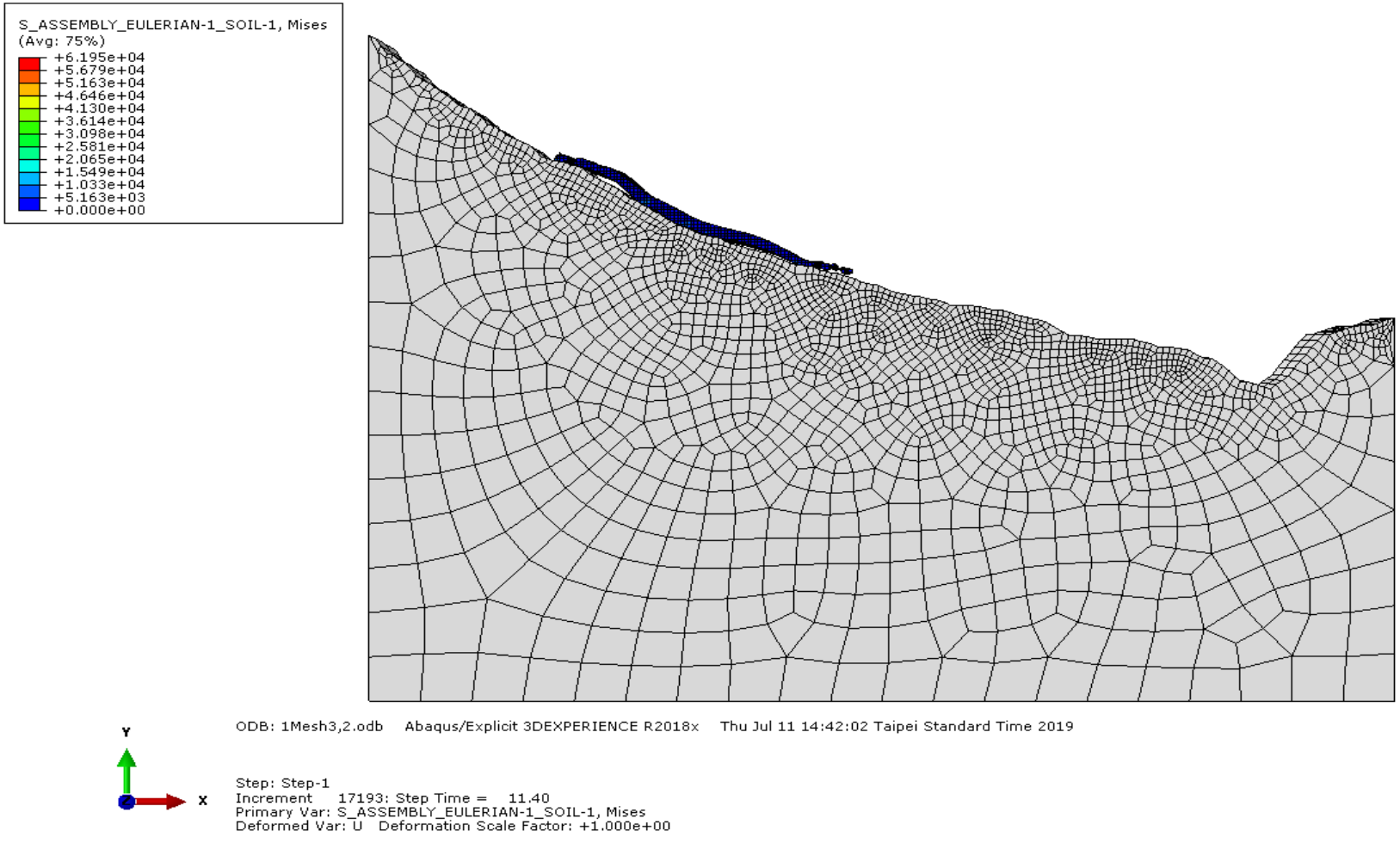

APPENDIX E-5: t = 19 s

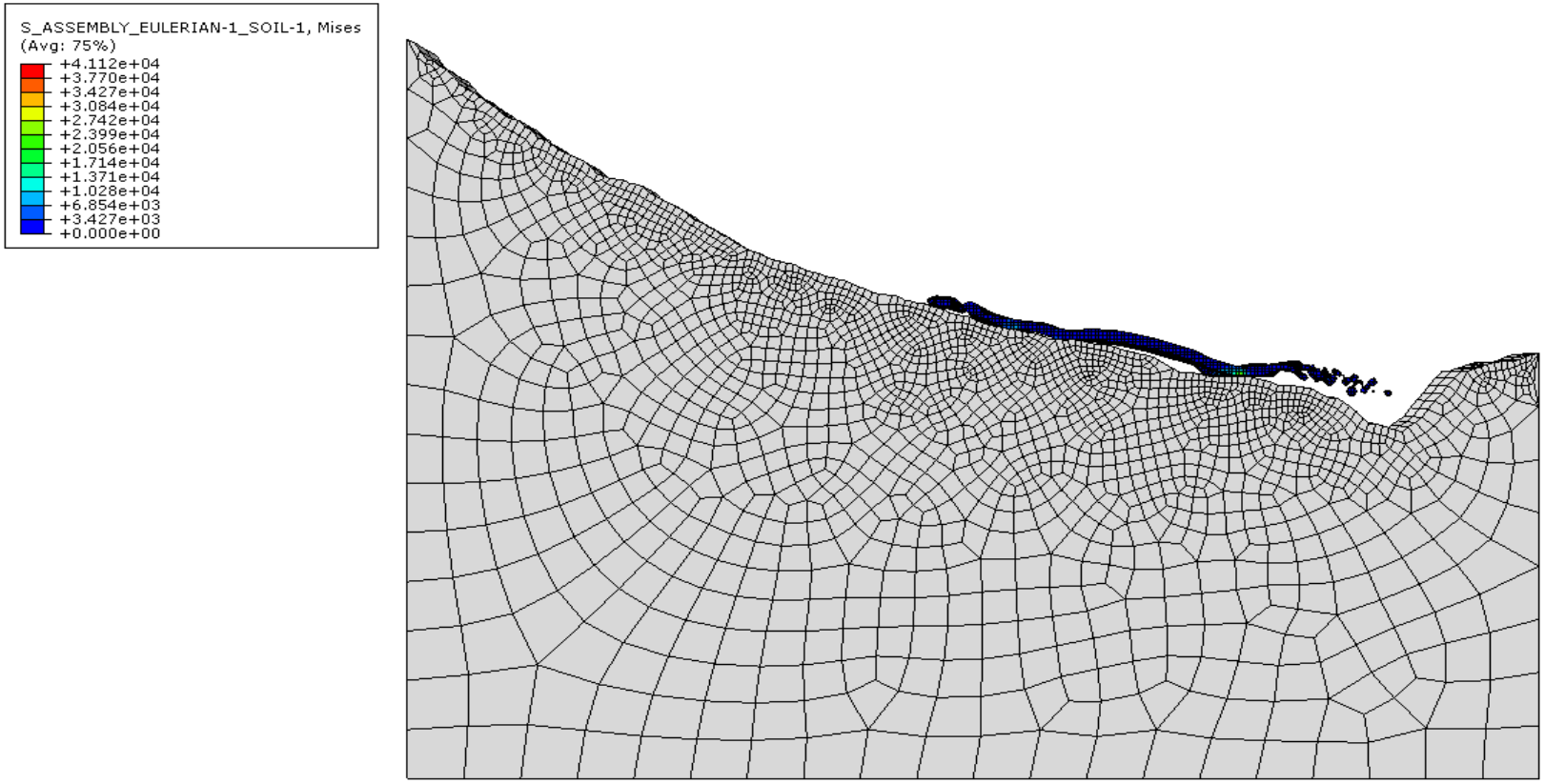

APPENDIX E-6: t = 20,90

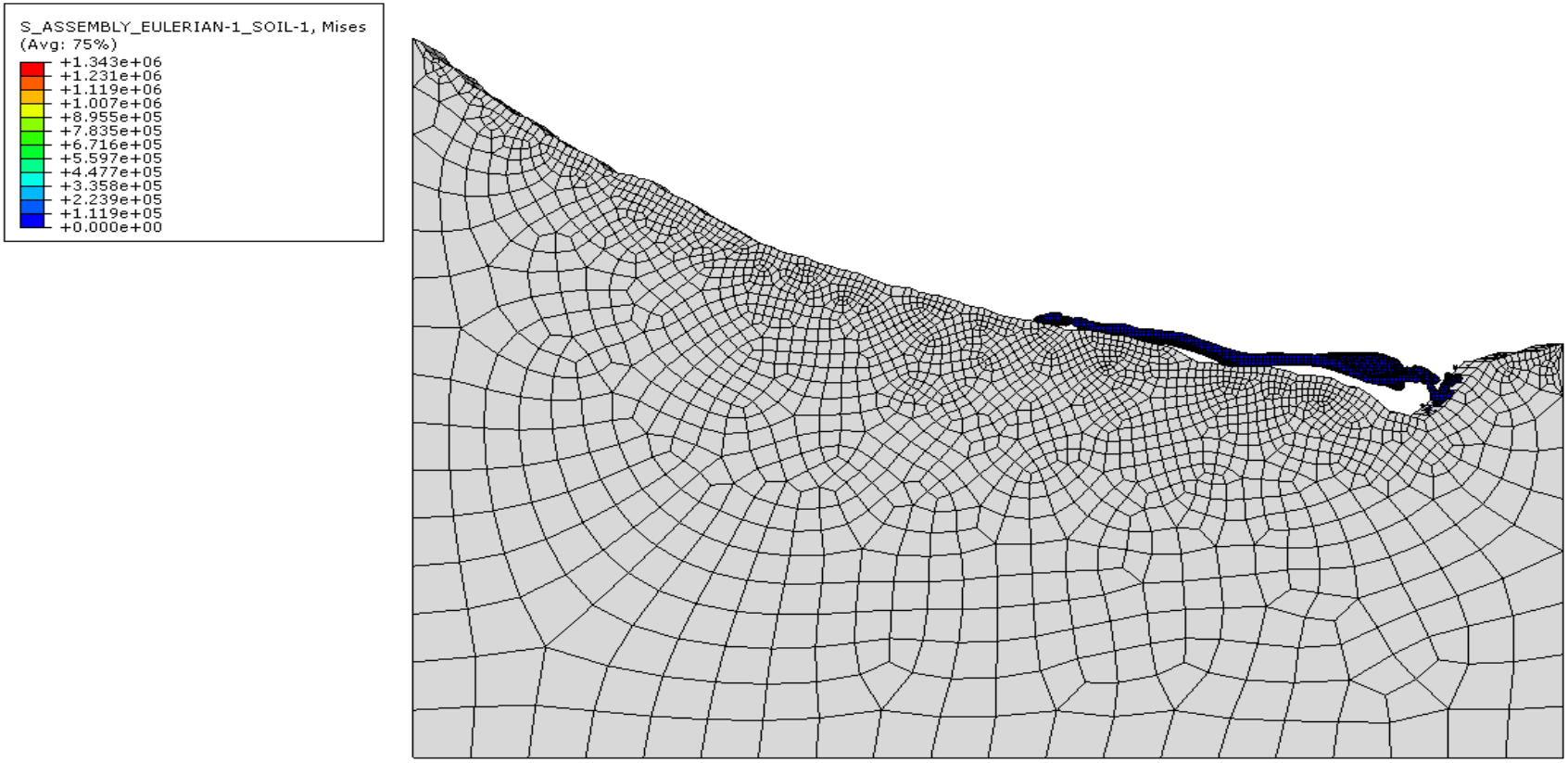

APPENDIX E-7: t = 38 s